International Journal of Education and Science Research Review
E-ISSN 2348-6457
Volume-7, Issue-6 December- 2020
P-ISSN 2349-1817
www.ijesrr.org
Email- editor@ijesrr.org

A BRIEF STUDY ON RHEOLOGY OF TWIST-GRAIN-BOUNDARY-A LIQUID CRYSTALS

Aditya Saini
Research Scholar
Deptt. of Physics
Malvanchal University
Indore (M.P.)

Dr. V. K. Suman
Research Supervisor
Deptt. Of Physics
Malvanchal University
Indore (M.P.)

ABSTRACT:- All types of materials may have their mechanical characteristics altered by the presence of structural defects or disorders. In substances, the disorder or flaws that are necessary for achieving desirable mechanical characteristics are formed or paralysed by impurities. Many asymmetrical fluids also including liquid crystals exhibit topological flaws. It is reasonable to anticipate that the network of flaws present in such systems will make a considerable contribution toward the rheological characteristics since they are able to respond to shear. The incorporation of nano zno into piezoelectric materials might result in an increase in the intensity of defects present in the crystalline [1–3]. In the lyotropic lamellar system, Basappa and colleagues demonstrated that introducing particles with a size of less than 9 micrometres increases the elastic moduli, and that the elasticity is mostly caused by the presence of defect networks [1].

KEYWORDS:- *Twist Grain, Liquid, Crystals, Boundary*

INTRODUCTION

Researchers Ramos and colleagues investigated the flowability of defect networking by distributing colloidal particles (1 m) into cholesteric liquid crystals. They discovered that the cholesteric phase exhibited a genetic condition solid behaviour [2]. Bandyopadhyay and colleagues have shown that the rigidity of LC-aerosil (7nm) hybrids of SmA liquid crystal (octyl cyanobiphenyl (8CB)) is improved in comparison to the pris- tine sample [3]. Wood et al. [4] lately reported an increase in the elasticity liquid liquid crystals that was caused by a network of defective lines that were entwined with colloidal particles. In most cases, the viscoelastic characteristics of such composite systems are improved, and their dynamics may be characterised using the theory of latex elasticity or the smooth.

However, fabrics with protracted periodic structural disorder caused by defects (dislocations) and the surface layer formed of an array of misalignments are uncommon, and the viscoelastic characteristics of these materials have not been well investigated. A type-II smectic-A liquid crystal, also known as a twist grain boundary-A

(TGBA) liquid crystal, is an example of this exceedingly uncommon kind of soft material. In this phase, the faults are intrinsic to the structure, and as a result, they may either be referred to as structural defects or intrinsic defects.

The twist bulk material phases, also known as TGBA, are dissatisfied phases that, in most cases, reside in the region that is intermediate between the cholesteric and the thermodynamically stable phases. The exact structure of all this phase is explained in chapter-1. The parallel between ferroelectric and smectic liquid crystals was initially stated by de Gennes [5], who anticipated one transition phase with a honeycomb of displacement in smectics. Renn and Lubensky demonstrated that the transition phase of substantially chiral aggregate concrete is composed of a distorted layout of blocks of SmA nanocrystals.

These blocks are separated from one another by twist grains, which are made up of an array of bolt dislocations [6, 7]. Goodby et al. [8] observed experimentally the contradictory organization of nematic layering or cholesteric-like twist in optically chiral crystal, and this structure was described by a number of studies [9, 10]. As soon because as discovery was made, there were various reports mostly on observation of numerous varieties of TGBA, such as TGBC and TGBC [10–12]. These reports came shortly after the discovery was made. In addition to the TGB phases, there is also a three-dimensionally modified chiral smectic-C phase that goes by the name UTGBC [13].

During the TGBA process, the grain boundary is formed by the interaction of dislocations, and the TGBA structure is stabilised by the interaction of grain boundaries with one another. The structure, techno characteristics, and dielectric properties of a variety of TGB liquid crystals have been the subject of a number of experimental investigations [13, 14]. The viscoelastic characteristics of this phase, on the other hand, have not been investigated. The rheological characteristics of the TGBA, UTGBC, and SmC phases are the topic of discussion in this section.

As a general rule, the TGBA phase only occurs within a very restricted temperature range; as a result, it is challenging to carry out the studies. It has been determined that the ambient temperature may be expanded by include both chiral and nonchiral molecules in the mixture, although in a specific ratio. In the course of this investigation, we created a binary combination that demonstrates a broad mean temperature of TGBA phase.

Experimental

We generated a binary combination by combining two different chemicals, namely 4-(2 -methyl butyl phenyl

4 - n-octylbiphenyl-4-carboxylate (CE8) and 2-cyano-4-heptyl-phenyl-4 -pentyl-4-biphenyl carboxylate [7(CN)5]. Both the chiral molecule CE8 and the nonchiral substance 7(CN)5 were synthesised by our colleagues in Poland. CE8 is chiral, but 7(CN)5 is not. Pramod et al. provided the detailed calibration curve of the binary mixes, which can be seen in Fig. 4.1 [12, 14].

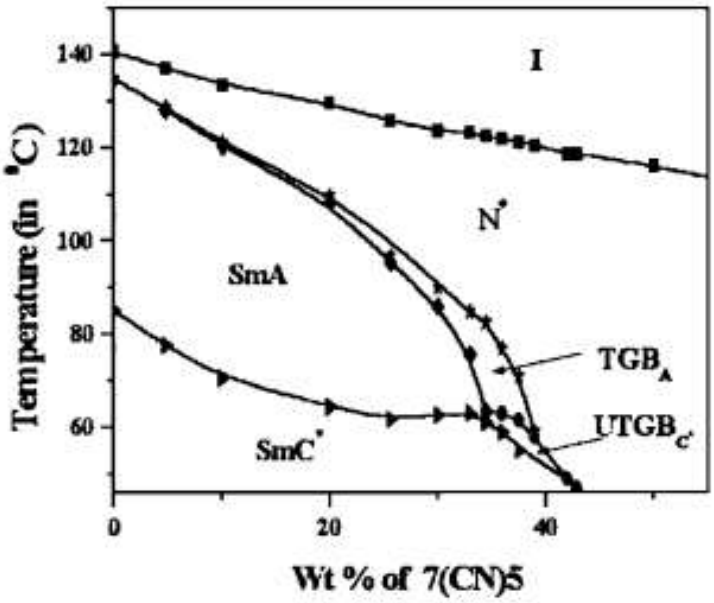

Figure: The phase diagram of the binary mixtures of CE8 and 7(CN)5. Adapted from ref. [12]

We made a homogeneous mixture by adopting 63.6 weight percent of CE8 and 36.4 weight percent of 7(CN)5 in order to acquire a broad ° c for the TGBA phase, which was based also on phase diagram shown above (Fig. 4.1). We heated the sample to a temperature that was higher than the bulk liquid, and then we mixed it physically using an extremely thin rod.

The following phase changes may be seen using a polarised optical microscope (POM) when the sample is cooled: I 120.2 °C; BP 119 °C; N 80 °C; TGBA 62.1 °C; UTGBC 59.8 °C; SmC 59.8 °C. It is important to note that the temperature gradient of TGBA is around 18 Celsius, but the air temperature of UTGBC is quite limited, approximately 2 Celsius. The temperature range that may be seen in TGBA is far wider than what is typically seen in a single thermochromic compound.

All of the rheological measurements were carried out with the assistance of a pain rheometer that had a cone and plate measuring system with a diameter of 25 millimetres, an angle of 1 degree on the cone, and a minimum

gap of 50 micrometres. After installing the sample, researchers heated it until it entered the isotropic phase. The next tests were carried out while the sample was allowed to cool. After that, the sample was presheared for around 400 seconds at a shear rate of 10 seconds per second before the measurements were taken.

Results and discussion

Texture and physical observations

First, we "carried out some preliminary research by placing the material in a planar cell and examining it using an optical polarising microscope (OPM). The characteristic textures of the several stages were noted by us, and they are shown in figure 4.2. The N phase features the characteristic defect architecture of the oily-streak (see Figure 4.2(a)). The TGBA phase has a very homogeneous texture, and the modest nonuniformity in colour may be attributed to the fact that the helix axis is not aligned uniformly across all areas ([Fig. 4.2(b)]).

In addition to this, we found that the UTGBC phase had a rather narrow temperature range below the TGBA phase and exhibited a distinctive square-grid layout. Further, we were able to see SmC by reducing the temperature, and this resulted in the continuation of the square and circular patterns [Fig. 4.2(c)]. This result may be eliminated by gently shearing the one of the plates.

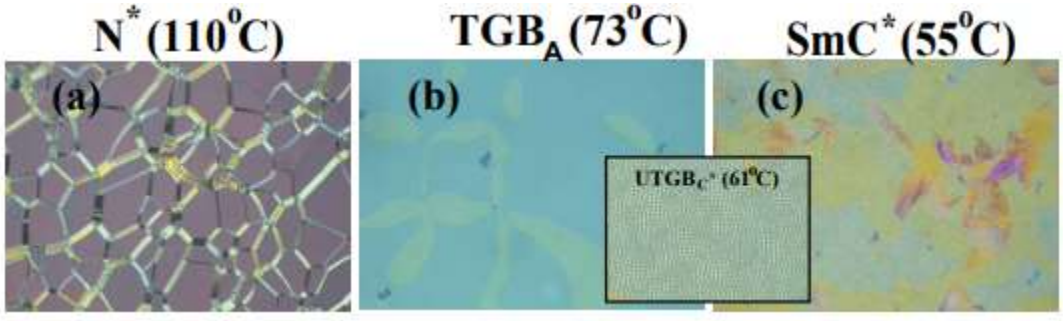

Figure: Textures observed under polarizing optical microscope (POM) at different temperatures (a) 110◦C (N ∗) (b) 73◦C(TGBA), and (c) 55◦C (SmC∗). A square grid pattern appears in between TGBA and SmC∗ phase indicating the UTGBC∗ phase, as shown in the box.

Figure 3.3 depicts, throughout a range of temperatures, the many ways in which the sample manifests its physical characteristics. This observation was carried out despite the presence of a mechanical interruption, such as the object being pulled up by a glass plate rod. It would seem that the N phase may be readily manipulated as a liquid would be. The TGBA component has the appearance of a viscous liquid, but the SmC

phase is more like a mid that fails to flow very smoothly.

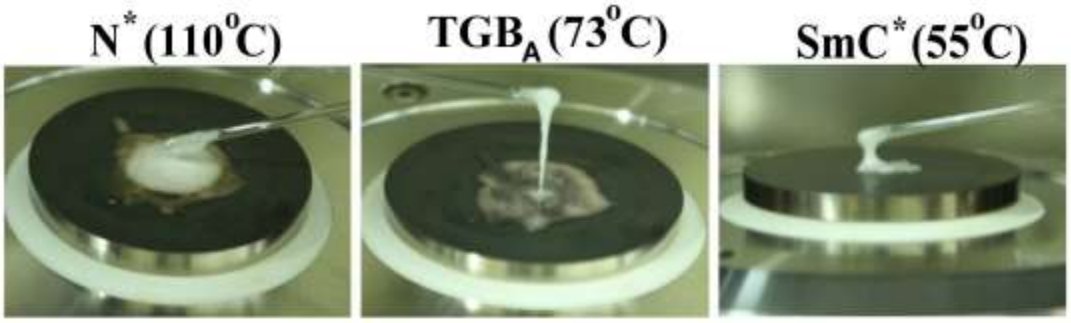

Figure: The physical appearance of the sample while trying to pull it up by a glass rod at different phases.

Rotational measurements

To begin, we carried out the temperature-dependent shear viscosity experiment at a constant shear rate of one hundred shears per second so that we could see all of the phase changes.

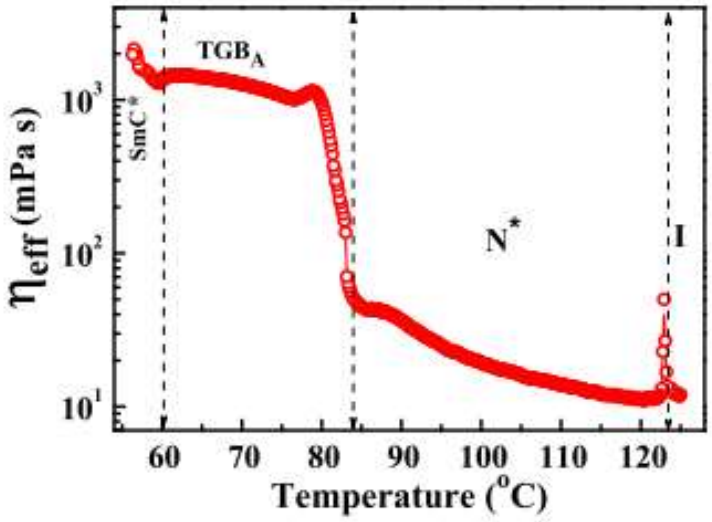

Figure: Variation of effective shear viscosity as a function of temperature at a constant shear rate 100 s−1.

Figure 3.4 depicts the temperature dependence of the shear viscosity, which allowed us to detect three different phase transitions: I 123 degrees Celsius N to 83.5 degrees Celsius TGBA 60 degrees Celsius SmC. When

compared to the crossover temperatures recorded under POM, these rates are just slightly different (within a range of 2 to 3 degrees Celsius). This is as a result of either the variation in the thermometer calibration or the surface temperature that the rheometer plate has.

In the cholesteric phase, we found that the viscosity rose gradually over time. This was something that we noticed. After then, there is a significant rise in the viscosity during the transition from N to TGBA, which is then followed by the SmC phase. Both the reasons for the significant rise in viscosity in the TGBA phase as well as the SmC phase will be explored later.

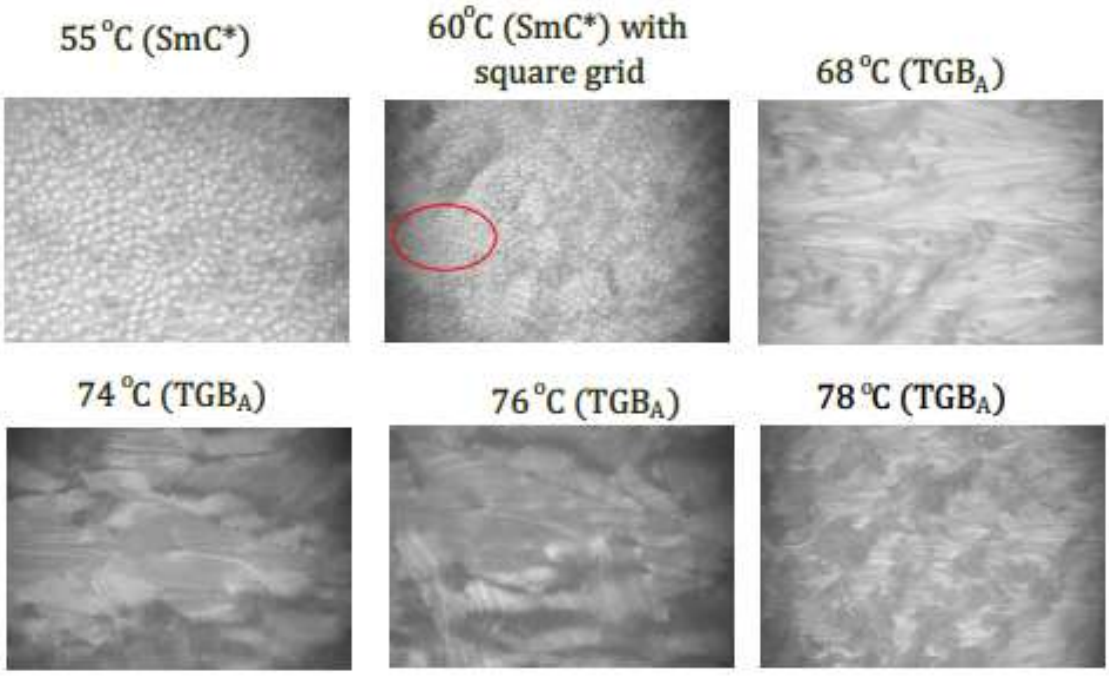

Figure: The simultaneous rheomicroscopy images are taken during the measure- ment of temperature dependant shear viscosity at a constant shear rate 100 s−1. The red circle shows the square grid patterns in the UTGBC∗ phase.

During the measurement of temperature-dependent shear viscosity, we carried out the synchronized rheomicroscopy scans at a constant shear rate of 100 s1; this allowed us to keep the temperature of the sample constant. Figure 4.5 provides a visual representation of the photos. At 55 degrees Celsius, a typical SmC roughness may be seen (unaligned). At 60 degrees Celsius, there are a few spots that look like square grid layouts, which indicates that the UTGBC phase is present.

After raising the temperatures once further, we saw that the textures were quite similar to the Grandjean orientation when the circumstances were planar anchoring [15]. These are some of the properties of the TGBA phase, which are shown in Fig. 3.5 (at temperatures of 68, 74, 76, and 78 degrees Celsius). It is likely that the quick rise in pitch value is to blame for the fact that the TGBA phase displays distinctively diverse textures depending on the temperature.

We carried out shear stress measurement that were dependent mostly on shear rate in order to get the apparent fracture toughness for the purpose of making relative comparisons between the various phases of something like the sample [16–18]. Figure 4.6 illustrates how the shear rate affects the effective applied load (eff) at a variety of temperatures.

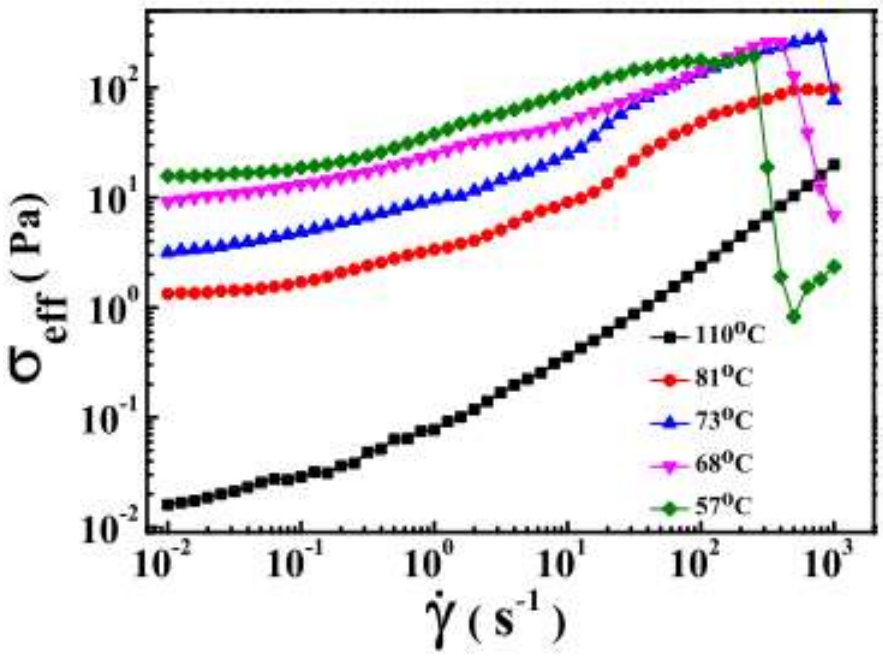

Figure: Shear rate dependent effective shear stress (σeff) at different tempera- tures N ∗: [110oC (squares)], near N ∗-TGBA transition: [81oC (circles)], TGBA: [73oC (uptriangles)], TGBA: [68oC (downtriangles)], SmC∗: [57oC (diamonds.]

peratures. When the shear rate is low (0.1 s1), the stress has a tendency to achieve virtually a set point as the shear rate approaches zero, which demonstrates a perceived yield stress (y). At a temperature of 110 degrees Celsius (N), the value of y is very low (y is less than 102 Pa), and it rises as the temperature falls in both the TGBA and SmC phases. For instance, y is less than 10 Pa when the temperature is 68 degrees Celsius (TGBA), but it rises to around 20 Pa when the temperature is 57 degrees Celsius (SmC) phase. The presheared sample

comprises a defect network consisting of residual oily streaks, which is the cause of the very tiny y in the N phase.

In this case, the value of y in the TGBA is three order of magnitude greater than that of the N phase. The determination of the apparent yield stress has also been reported in a great number of different types of smectic liquid crystals [19, 20]. However, the perceived yield point of the TGBA and the SmC phases of the current framework is much higher than the fracture toughness that is known at low weight smectic microcrystals [19, 21]. At large shear rates (more than 10 s1), the N phase demonstrates shear thinning, which is thereafter followed by a Newtonian behaviour. In the range of shear rates that are considered intermediate, that is, between 0.1 and 100 s1, it exhibits shear thinning behaviour in all of the phases.

The Reissner number [22] is typically used to characterise the sheer fucking various parameters viscosity of randomly oriented or cholesteric liquid crystals. This number is determined by the ratio of something like the rhythm viscous stress ( ) to the Edward stress (K/h2), within which K is the median income curvature elasto - plastic constant but instead h is the size scale of the flow geometry.

Essentially, it has been proven that the shear viscosity displays a shear thinning tendency [23] in the appropriate position of the Reissner number (10 to 400). This range of the Pseudo - second - order number is between 10 and 400. Assuming a standard expected price of curvature flexible constant K = 1011 N and plastic viscosity of the N + phase = 10 mPa s, the computed Ericksen figure is around 300, which falls within the range of values that have been theoretically anticipated. When the shear rate is very high (> 100 s1), the eff value in both the TGBA and SmC phases drops precipitously to a much lower value. This unexpected drop might be the result of the wall slipping or the sample's ductile materials.

Oscillatory measurements

We investigated the strain level dependency of storage (G) and loss (G) moduli at a range of temperatures in order to ascertain whether or not viscoelasticity behaves in a linear fashion. The measurement is carried out each time on a newly collected specimen, and the outcomes are displayed in Figure 4.7.

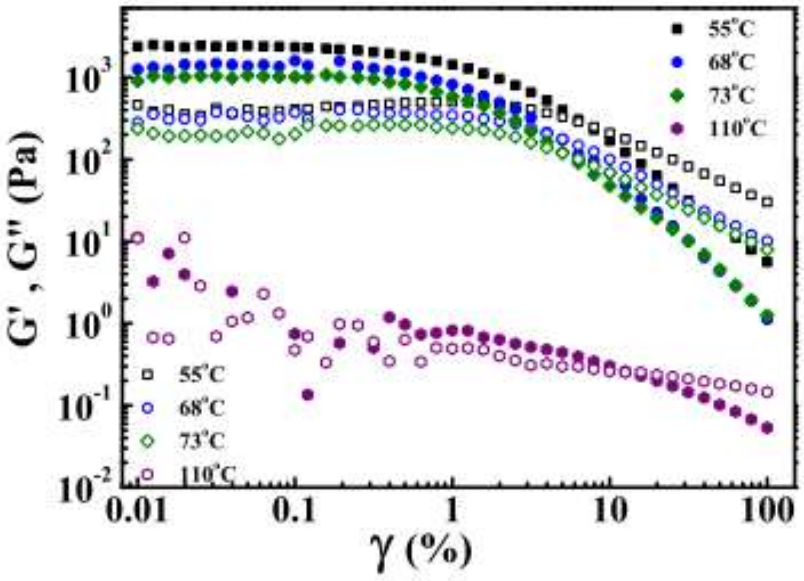

Figure: The strain amplitude dependence of the storage G (solid symbols) and the loss G*jj* (open symbols) moduli at different temperatures. 110◦C (hexagons) [N ∗], 73◦C (diamonds) [TGBA], 68◦C (circles) [TGBA], and 59◦C (squares) [SmC∗] at ω = 1 rad/s.]

Due to the lowest limit of the Gj and Gjj values that our metre can reproducibly measure, the results at low strain volume in the N phase at 110 degrees Celsius are noisy. (73 degrees Celsius and 68 degrees Celsius) in the linear viscoelastic area of the TGBA phase, Gj > Gjj, and Gj of TGBA is more than a thousand times bigger than that of the N phase. In a similar manner, the value of j jj and Gj in the SmC phase (at a temperature of 55 degrees Celsius) is about 2.5 times greater that of the TGBA phase. The dual network of persistent oily-streak defects [2] is primarily responsible for the majority of the viscoelasticity that is shown by the N phase.

Because of the temporal order, SmA liquid crystals exhibit a greater viscoelastic responsiveness than nematic or N liquid crystals do. For instance, in our earlier research, we discovered that cholesterol nonanoate (which shows the N to the SmA transition) has a GSmA that is lower than 80 GN [24]. In the sample that we have here, we discovered that GT GBA is more than 1000 GN. As a result, the increased suppleness of the TGBA phase may be explained by attributing it to the structural faults that are already present throughout the system. In this phase, the increase in deformability may be due to the fuel costs for the displacement of grain boundaries, which is an additional possible explanation. In addition, the air pressure of the cubic crystal layers, which works against the strain, plays a critical role in raising the shear modulus. This tension serves as a brake on the material's ability to deform. Although there are no grain boundaries in the SmC phase, the viscoelastic characteristics are

still influenced by the individual imbalances and how they move.

In point of fact, it has been hypothesised that the shear modulus is significantly affected by the symptoms . people of screw dislocations. This is due to the fact that the column tension opposes the Peach-Koehler attraction, which is the factor that regulates the velocity of the screw displacement [25]. The system is said to have transcended its deflections and to be undergoing plastic deformation because when force that is placed on the deformations is dominant over the line tension.

It's possible that the plastic deformation is to blame for the significant decrease in eff that's seen in Fig. 4.6 for both the TGBA and SmC phases. Numerous writers [1, 3, 25–31] have examined the influence that defects and disorder have on the rheological of particles type-I smectic water crystals. In those trials, the flaws were either stabilised by quenching the disorder or by spreading colloidal particles throughout the samples. Both of these methods were successful in achieving the desired results. The storage modulus of these types of devices exhibits a behaviour that is described by a power law [2, 3].

$$G'(\omega) = G_{\circ} + \beta\omega^{\alpha}$$

where G represents the plateau modulus that is derived from the low frequency region shear modulus. Grain boundaries are brought about as a result of the fact that the TGBA in this sample is made up of spinning SmA blocks. These flaws are a natural characteristic of the structure and cannot be eliminated with the application of shear force. In this section, we use the power-law model to conduct an analysis of the dynamic characteristics of our sample (Eq. 3.1).

In each of the phases, some example frequency dependences of storage and loss moduli are shown in Figure 4.8. Throughout the N phase, Gj is greater than Gjj, and both values remain constant during the low frequency zone (2 rad/s). Once you go outside of this frequency range, they become more frequent. For instance, after you get above a speed of 2 rad/s, the values change to Gj 2 and Gjj . In the low frequency zone (= 1 rad/s), solid-like behaviour was also seen in colloidal-particle-dispersed cholesteric liquid crystals, which is something that should be highlighted.

However, when the frequency was increased, the same sample exhibited behaviour similar to that of a fluid (G G) [2]. The parameters of the fit that were collected from the various stages are shown in Fig. 3.9. (a). During the N phase (90 to 110 degrees), the values of derived from the Gj and Gjj data are virtually identical to the

numbers 2 and 1, respectively. It is important to observe that the exponent derived from the fits of Gj and Gjj is virtually identical, which means that 0.5. This is the case since the exponent falls fast (below 90 degrees Celsius). Ramos et al. [2]

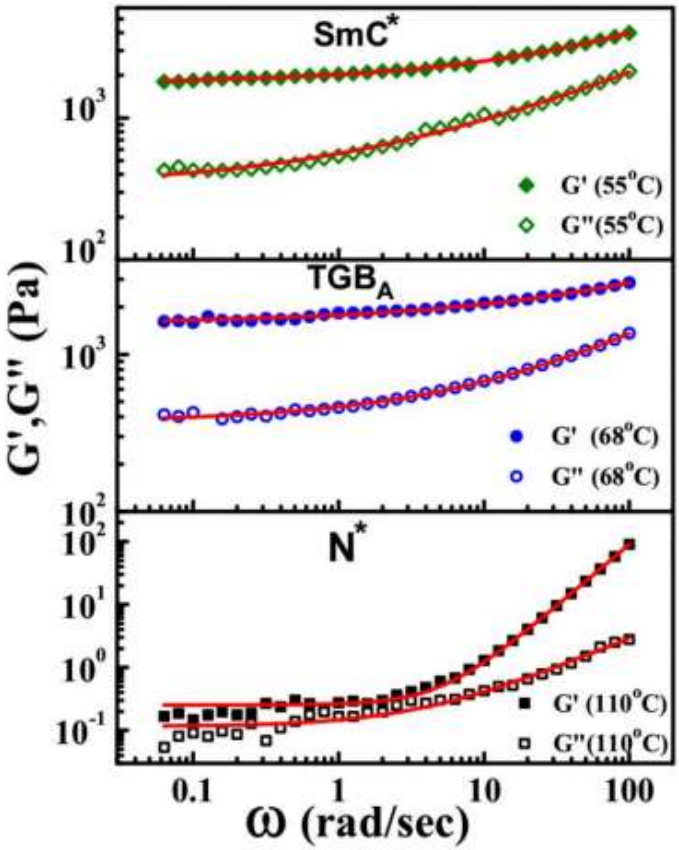

Figure 4.8: The frequency dependence of (a) storage G (solid symbols) and (b) loss G (open symbols) moduli at three representative temperatures in all the phases. The solid lines are best fits to Eq. (3.1).

shown that the storage capacity of highly crystalline systems that include a defect network receives contributions simultaneously from the confused section of the sample, Gj () a 1/2, and from parts of the sample where its layers are orthogonal to the stress direction, Gj () a 2.

In a same manner, the loss modulus contains contributions from both disoriented regions of the sample (represented by the expression Gjj () a 1/2) and a Maxwell fluid type (represented by the expression Gj () a). In light of our findings, it would seem that the memory and loss properties of the TGBA phase get a major contribution just from the layer of the sample that are not orientated in a particular direction.

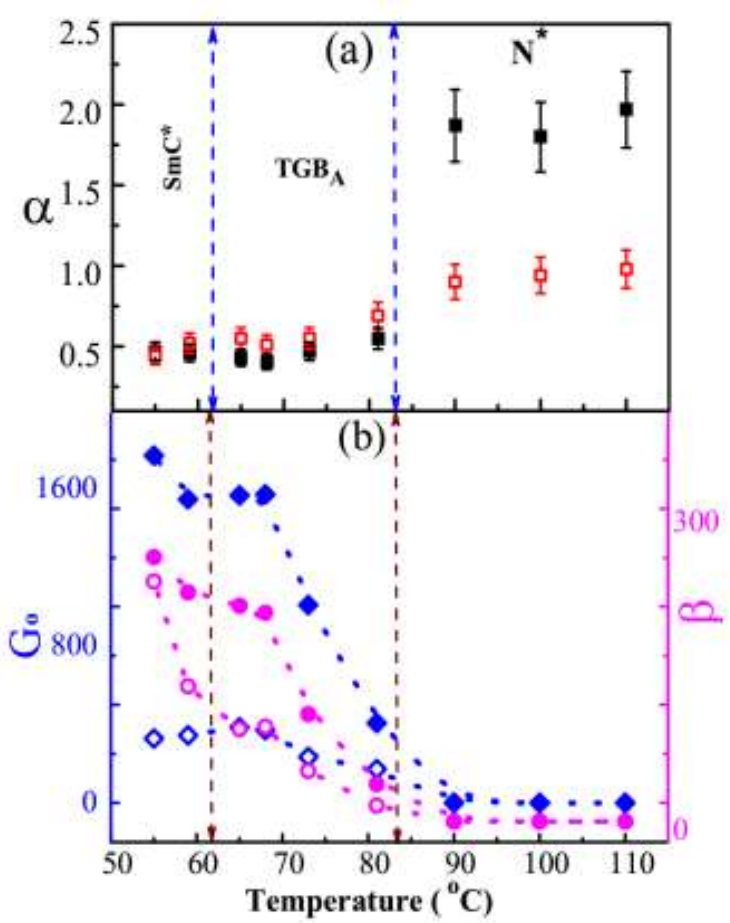

Figure 4.9: (a) The exponent α characterizing the power-law contribution to G (ω)(solid squares) and G (ω) (open squares) as a function of temperature. (b) Tem- perature variation of fit parameters, G◦ and β obtained from the fitting of G (ω) and G (ω) data. Diamonds (solid and open) and circles (solid and open) are obtained from G (ω) and G (ω) data respectively.

The temperature dependence of G◦ and β obtained from the fitting of G$_j$ (ω) and G$_{jj}$ (ω) is also shown in Fig. 4.9(b). For example, at 110◦C, G◦ obtained from both the fits are 0.25 and 0.12 respectively.

At the same temperature, β values are 0.01 and 0.03 respectively, and similar values were also reported in other cholesteric samples [2]. The plateau modulus (G◦) usually arises from the elasticity of static defects in lamellar systems [2, 3]. In the present system G◦ is much larger (≃ 10 times) than the low molecular weight thermotropic SmA liquid crystal, such as 8CB [3].

The variation of G◦ with reduced temperature $\chi \equiv (TN* - T\ GBA\ -T)/TN* - T\ GBA$ is shown in Fig. 4.10. In the

TGBA and SmC∗ phases, G◦ is more than three orders of magnitude larger than the N ∗ phase [2]. In analogy with rubber elasticity, the contribution to the elastic response of static defect network varies as G◦ ≈ τ /d2, where τ is the line tension and d is a typical average spacing between defects [2]. In case of screw dislocations the defect line tension can be written as $\tau = Bb_c^4/128\pi 3r2$, where B is the layer compression modulus, b = md◦ is the Burger's vector of integer strength m and rc is the defect core radius [32].

Measurements on many smectic systems show that B ∼ χ0.4 [33] and r−2 ∼ ψ2 ∼ χ0.5, where ψ is the smectic order parameter [34]. Hence the defect line tension (τ) can be defined as, τ ∼ χ0.9, which implies G◦ ∼ χγ with γ ≈ 0.9. It suggests the defects significantly contribute to the shear response [34]. In analogy with this theoretical calculation we have fitted χ dependent G◦ values with respect to the equation G◦ ≃ χγ (Fig. 4.10), which shows the fitting parameter γ = 1. It is comparable with the theoretical calculation, suggesting the screw dislocations notably contribute to the shear response . Assuming a moderate

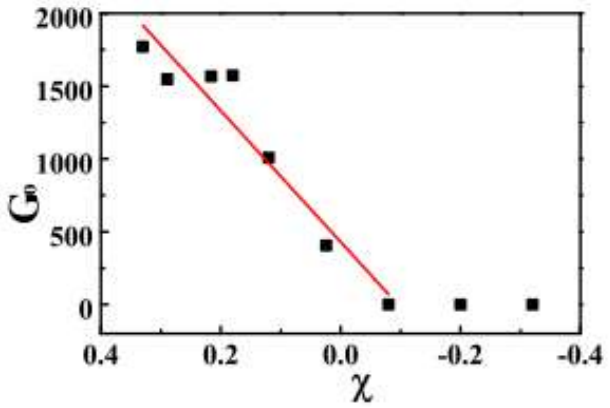

Figure 4.10: The variation of G◦ with reduced temperature χ. The solid line showing the best-fit result G◦ ≃ χγ , with γ = 1

The plotted as a function of Gj and Gjj, which was derived by fitting Gj () and Gjj (), may also be seen in Fig. 4.9. (b). For instance, the G values derived from the two fits for 110 degrees Celsius are 0.25 and 0.12 respective. The values are 0.01 and 0.03 sequentially at the same latitude, and comparable values were previously reported in other organization are as follows samples [2]. The plateau modulus, denoted by the symbol G, is often derived from the stiffness of the static flaws that are present in dendritic systems [2, 3]. In the current setup, G has a magnitude that is about ten times greater than the low molecule weight highly crosslinked SmA liquid crystals, such as 8CB. [3].

Figure 4.10 illustrates how the value of G changes when the temperature drops, as shown by the formula (TNT GBA -T)/TNT GBA. In both the TGBA and SmC phases, the difference in size between G and N is greater by more nearly three orderings of magnitude [2]. The contributions to the deformation of a static defective network changes according to the formula G /d2, where is the line tensions and d is an average normal spacing amongst defects [2].

This formula is based on an analogies with the rigidity of rubber. The flaw line tension may be expressed as = Bb4/1283r2 in the condition of screw displacement, where B has become the layer compressing modulus, b = md is the Sandwich's vector of numeric strength m, and rc is just the defects core radius [32]. In several smectic systems, measurements have shown that B is less than 0.4 [33] and that r2 2 is less than 0.5 [34], where is the thermodynamically stable order parameter. Therefore, the defect column tension () may be defined as, 0.9, which means that G with 0.9 when is less than 0.9. This leads one to believe that the flaws have a substantial role in the shear response [34]. In accordance with this simulated results, we have adapted dependent G numbers with regard to the solution G (Fig. 4.10), which demonstrates that the fitting parameter = 1 is appropriate. It is consistent with the theoretical estimate, which suggests that the screw downturns contribute significantly to the shear response. Taking into account a typical

CONCLUSION

The rheological properties of a reaction mixture that exhibited a broad temperature range for the TGBA phase was investigated by us. Solid-like behaviour may be seen from each of the phases present in the mixture, which are denoted by the symbols N, TGBA, and SmC respectively. On the basis of the concept of lamellar systems, which takes into consideration the contribution of flaws, a discussion is held about the stiffness of the TGBA phase.

Both the power-law sensitivity of the composite fracture toughness and the interpretation of the findings of the experiments point to the design deficiencies as the cause of the higher suppleness of the TGBA phase. The active noise level is getting closer to 1, which suggests that TGBA semiconductor materials and its phases that form at low temperatures are a genetic condition soft solid that dynamics is comparable to that of soft glassy materials.

REFERENCES:-

1. Acharya, A., & Dayal, K. (2013). Continuum mechanics of line defects in liquid crystals and liquid

crystal elastomers. *Quarterly of Applied Mathematics*, *72*(1), 33–64. https://doi.org/10.1090/s0033-569x-2013-01322-x

2. Basappa, G., Suneel, Kumaran, V., Nott, P. R., Ramaswamy, S., Naik, V. M., & Rout, D. (1999). Structure and rheology of the defect-gel states of pure and particle-dispersed lyotropic lamellar phases. *European Physical Journal B*, *12*(2), 269–276. https://doi.org/10.1007/s100510051004

3. Cao, M., Liu, S., Zhu, Q., Wang, Y., Ma, J., Li, Z., Chang, D., Zhu, E., Ming, X., Liu, Y., Jiang, Y., Xu, Z., & Gao, C. (2022). Monodomain Liquid Crystals of Two-Dimensional Sheets by Boundary-Free Sheargraphy. *Nano-Micro Letters*, *14*(1), 1–13. https://doi.org/10.1007/s40820-022-00925-2

4. Čopar, S., Kos, Ž., Emeršič, T., & Tkalec, U. (2020). Microfluidic control over topological states in channel-confined nematic flows. *Nature Communications*, *11*(1), 1–10. https://doi.org/10.1038/s41467-019-13789-9

5. Everts, J. C., & Ravnik, M. (2021). Ionically Charged Topological Defects in Nematic Fluids. *Physical Review X*, *11*(1), 11054. https://doi.org/10.1103/PhysRevX.11.011054

6. Fadda, F., Gonnella, G., Lamura, A., Orlandini, E., & Tiribocchi, A. (2018). Rheology of an inverted cholesteric droplet under shear flow. *Fluids*, *3*(3), 1–14. https://doi.org/10.3390/fluids3030047

7. Krakhalev, M. N., Bikbaev, R. G., Sutormin, Timofeev, I. V., & Zyryanov, V. Y. (2019). Nematic and cholesteric liquid crystal structures in cells with tangential-conical boundary conditions. *Crystals*, *9*(5), 28–39. https://doi.org/10.3390/cryst9050249

8. Kumar, N., Zhang, R., De Pablo, J. J., & Gardel, M. L. (2018). Tunable structure and dynamics of active liquid crystals. *Science Advances*, *4*(10), 1–13. https://doi.org/10.1126/sciadv.aat7779

9. Li, C. Y., Wang, X., Liang, X., Sun, J., Li, C. X., Zhang, S. F., Zhang, L. Y., Zhang, H. Q., & Yang, H. (2019). Electro-optical properties of a polymer dispersed and stabilized cholesteric liquid crystals system constructed by a stepwise UV-initiated radical/cationic polymerization. *Crystals*, *9*(6), 20–27. https://doi.org/10.3390/cryst9060282

10. Mitov, M. (2020). Advances in Cholesteric Liquid Crystals. In *Advances in Cholesteric Liquid Crystals*. https://doi.org/10.3390/books978-3-03928-229-6

11. Ramos, L., Zapotocky, M., Lubensky, T. C., & Weitz, D. A. (2002a). Rheology of defect networks in cholesteric liquid crystals. *Physical Review E - Statistical Physics, Plasmas, Fluids, and Related Interdisciplinary Topics*, *66*(3), 1–38. https://doi.org/10.1103/PhysRevE.66.031711

12. Ramos, L., Zapotocky, M., Lubensky, T. C., & Weitz, D. A. (2002b). Rheology of defect networks in cholesteric liquid crystals. *Physical Review E - Statistical Physics, Plasmas, Fluids, and Related Interdisciplinary Topics*, *66*(3). https://doi.org/10.1103/PhysRevE.66.031711

13. Varney, M. C. M., Jenness, N. J., & Smalyukh, I. I. (2014). Geometrically unrestricted, topologically constrained control of liquid crystal defects using simultaneous holonomic magnetic and holographic optical manipulation. *Physical Review E - Statistical, Nonlinear, and Soft Matter Physics*, *89*(2), 1–12. https://doi.org/10.1103/PhysRevE.89.022505

14. Yu, C. H., Wu, P. C., & Lee, W. (2019). Electro-thermal formation of uniform lying helix alignment in a cholesteric liquid crystal cell. *Crystals*, *9*(4), 62–71. https://doi.org/10.3390/cryst9040183

15. Zakri, C., Blanc, C., Grelet, E., Zamora-Ledezma, C., Puech, N., Anglaret, E., & Poulin, P. (2013). Liquid crystals of carbon nanotubes and graphene. *Philosophical Transactions of the Royal Society A: Mathematical, Physical and Engineering Sciences*, *371*(1988). https://doi.org/10.1098/rsta.2012.0499

16. Zhang, Q., Zhang, R., Ge, B., Yaqoob, Z., So, P. T. C., & Bischofberger, I. (2021). Structures and topological defects in pressure-driven lyotropic chromonic liquid crystals. *Proceedings of the National Academy of Sciences of the United States of America*, *118*(35). https://doi.org/10.1073/pnas.2108361118